ACS OMEGA

http://pubs.acs.org/journal/acsodf

Article

Computational and Biophysical Characterization of Heterocyclic Derivatives of Anthraquinone against Human Aurora Kinase A

Mandeep Singh, Md. Anzarul Haque, Alexander S. Tikhomirov, Andrey E. Shchekotikhin, Uddipan Das, and Punit Kaur*

Cite This: *ACS Omega* 2022, 7, 39603−39618

Read Online

ACCESS | Metrics & More | Article Recommendations | Supporting Information

ABSTRACT: Human Aurora kinase A (AurA) has recently garnered the attention of researchers worldwide as a promising effective mitotic drug target for its involvement in cancer and related inflammatory anomalies. This study has explored the binding affinity of newly identified heteroarene-fused anthraquinone derivatives against AurA. Molecular docking analyses showed that all the heteroanthraquinone compounds bind to AurA with different affinities. Molecular dynamics simulation studies revealed that the compounds maintained relatively stable binding modes in the active site pocket while inducing minimal conformational changes in the AurA structure, interacting with key residues through several noncovalent interactions, including hydrogen bonds. Fluorescence spectroscopy and biolayer interferometry binding assays with synthesized compounds against recombinantly expressed AurA further verified their binding efficacy. Naphthoisatine **3** proved to be the best binder, with compounds anthraimidazole **5** and anthrathiophene **2** showing comparable results. Overall, this study indicates decent binding of heterocyclic derivatives of anthraquinone with the target AurA, which can further be assessed by performing enzymatic assays and cellular studies. The studies also highlight the applicability of the heteroarene-fused anthraquinone scaffold to construct selective and potent inhibitors of Aurora kinases after necessary structural modifications for the development of new anticancer drugs.

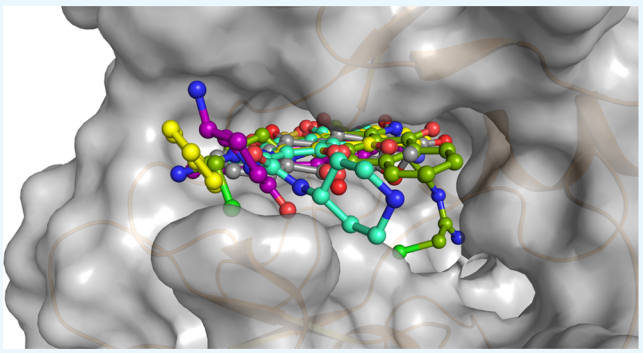

1. INTRODUCTION

The process of centrosome amplification is considered a "hallmark" of cancer cells and is commonly accompanied by chromosome segregation activity in the mitotic cell cycle. The phases in the cell cycle are firmly controlled through mitotic kinases, among which the Aurora kinase family, comprising human Aurora kinase A (AurA), human Aurora kinase B (AurB), and human Aurora kinase C (AurC), ensure the precise progression of cells into mitosis by not only aiding in the formation of a bipolar mitotic spindle but also through accurate segregation of chromosomes and the accomplishment of cytokinesis.[1−5] In particular, AurA has been known to play an essential role in various cellular processes, including the entry of cells in mitosis, chromosome derangement and alignment, separation and maturation of centrosomes, correcting spindle assembly, asymmetric division, and cilia dynamics. In contrast, its aberrant overexpression has frequently been correlated with tumorigenesis.[1,6−10]

The AurA gene is situated on human chromosome 20q13 and translates a 403 amino acid-long protein. This region of the chromosome has been observed to be amplified in an assortment of human tumors. The AurA gene itself is revealed to be amplified in >50 and >12% of primary colorectal and breast tumors, respectively, as well as in prostate, colon, ovarian, and cervical tumor cells.[11−15] The translated protein has also been observed to overexpress, resulting in elevated kinase activity in several tumor types.[8,16] In cancerous cells, the AurA protein has been known to overexpress and localize mutually in the nucleus as well as in the cytoplasm, irrespective of their cell-cycle phases.[17] The interactions between AurA and tumor suppressor p53 have frequently been linked to uncontrolled cell growth, while its inhibition through modulatory compounds has been postulated to trigger the activity of p53, which further leads to proliferation arrest and senescence in melanoma cells.[18−20] Overexpression of AurA has also been documented to increase genomic instability and aneuploidy by interrupting cell-cycle checkpoints while supporting cancer cell endurance and chemoresistance by activating the PI3K/Akt/GSK3 signaling cascade.[8,21,22] Hence,

Received: February 4, 2022
Accepted: October 7, 2022
Published: October 27, 2022

https://doi.org/10.1021/acsomega.2c00740
ACS Omega 2022, 7, 39603−39618

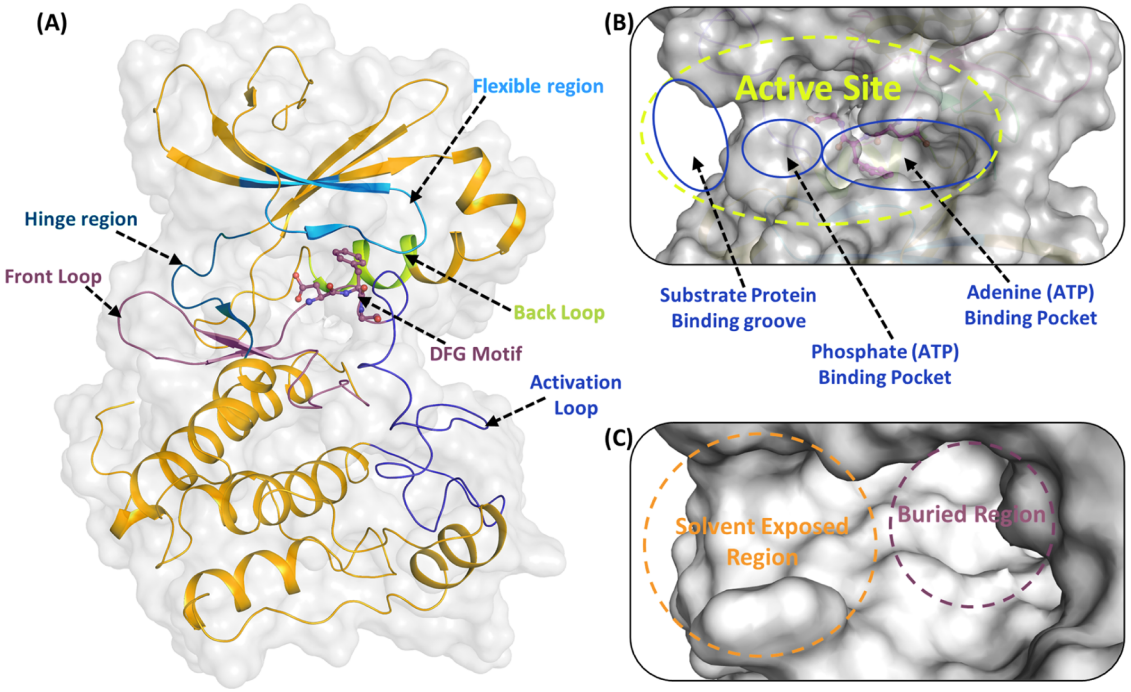

Figure 1. (A) Cartoon structure of AurA, together with the surface representation, indicating structural components of its catalytic kinase domain. (B) Surface representation of the AurA active site, indicating regions of ATP and substrate binding. (C) Surface representation of the AurA active site, highlighting its solvent exposed region and buried region. The above-displayed figures have been generated utilizing the crystal structure coordinates of PDB ID: 3H10.

modulation of AurA activity has been deemed an essential approach to effective anticancer therapy.

The human Aurora protein kinase family (AurA, AurB, and AurC) all have a highly conserved ATP binding pocket; that is, the catalytic domain of AurA shares numerous features with AurB and AurC.[23] All Aurora kinases majorly comprise three prominent domains with a single large binding site cavity. The Aurora kinases' catalytic domain consists primarily of a conserved C-terminal α-helical domain (residues 216−385) and a short N-terminal β-strand domain (residues 127−215) connected by a small hinge region (residues 210−215) that forms part of the active site (Figure 1A). In AurA, the catalytic domain containing the ATP binding active site encompasses five regions: a kinase hinge region which accommodates its heteroaromatic core (adenine), a ribose binding region, a solvent accessible region, a buried region (back pocket), and a phosphate-binding region that outspreads to the activation loop (residues 274−299) (Figure 1A,B,C).[24] The buried region is mostly involved in hydrophobic contacts, while the solvent-accessible region can make polar interactions aiding the fixation of potential inhibitors in a specific conformation (Figure 1B,C). The most important region is the hinge region, where a direct hydrogen-bonding network can be forged between adenosine (or other substrates) and residues within the hinge region, which in turn contributes significantly to the binding affinity of potential inhibitors.[24−27]

ATP is a co-substrate of these kinases required for the transfer of its γ-phosphate group to the hydroxyl groups of its target substrates, consequently altering their function. Hence, most of the reported inhibitors of Aurora kinases are structural analogues of ATP. While the ATP binding pocket is evolutionarily conserved, considerable distinct disparities exist in their active site residues. In AurA, the Leu215, Thr217, and Arg220 catalytic triad residues are substituted with Arg159, Glu161, and Lys164 residues in AurB, close to the solvent-accessible region of the protein (Figure 1C). Numerous findings have indicated that targeting these differential residues present in the binding pocket can help achieve enhanced selectivity for the inhibition of either of the kinases.[27,28] This subtype selectivity was excellently demonstrated through varied interactions of the indirubin-based inhibitors with the Thr217/Glu161 catalytic triad residue of AurA/AurB, respectively.[29]

Although quite a few Aurora kinase inhibitors have been studied at various phases of clinical trials, none has passed the criteria completely to be used as an effective anticancer therapeutic. The majority of these inhibitors failed to pass phase I/II of clinical trials due to various side effects, including toxicity.[27,30] Only a handful of AurA inhibitors have exhibited some promising results. Among them, the AurA-selective inhibitor molecule MLN8237 (Alisertib) is, to date, the most actively pursued lead, having undergone phase III clinical trials in various clinical settings.[27,28] Nevertheless, the advent of tumor cell resistance and organ toxicity remains the major restricting factor for achieving the desired efficacy from these inhibitors.

Recently, the anthraquinone scaffold has been extensively sought as a viable source for designing novel antitumor efficacious therapeutics. In particular, the various side-chain modifications of this scaffold have demonstrated enhanced inhibition of wild-type tumor cells, their altered drug response counterparts, and in various *in vivo* settings.[31−36] Other chemical modifications aimed at optimizing their physicochemical and chemotherapeutic properties have identified promising new preclinical candidates.

Further studying the chemotype of antitumor heteroarene-fused anthraquinones, we identified various anthraquinone scaffold-based compounds, among which best-in-series de-

https://doi.org/10.1021/acsomega.2c00740
ACS Omega 2022, 7, 39603−39618

rivatives were anthra[2,3-*b*]furan-3-carboxamides (e.g., anthrafuran **1**), possessing a multitarget antitumor effect with the ability to inhibit phosphorylation of proteins by the kinase AurB.[31,34,37−39] In this study, the top lead compounds obtained from previous studies have been tested for their *in silico* and *in vitro* binding capabilities against another important target belonging to the Aurora kinase family of enzymes, AurA.

2. METHODOLOGY

2.1. Molecular Docking. The three-dimensional (3D) structural coordinates of human AurA with the co-crystallized inhibitor 9-chloro-7-(2,6-difluorophenyl)-*N*-{4-[(4-methylpiperazine-1-yl)carbonyl]phenyl}-5*H*-pyrimido[5,4-*d*][2]-benzazepine-2-amine (97B) were retrieved for docking analysis (PDB ID: 3H10).[40] Docking studies of compounds with target AurA were performed after contemplating the active site amino acid residues and the location of the inhibitor (97B) inside the binding cavity. Before docking, the AurA protein was prepared using the Protein Preparation Wizard module in Maestro.[41] The Protein Preparation Wizard module step optimizes the overall hydrogen bonding environment, removes defined crystal waters, helps in filling any missing sidechains and loops using Prime, generates protonation and charge states for protein residues and bound ligands (pH 7.0 ± 2.0), and performs restraint energy minimization on the macromolecular structure.[42] Taking the centroid of the bound inhibitor 97B, various grids (5−15 Å) that characterized a cube, where the ligand molecule was suggested to bind, were created. Two-dimensional (2D) structures of compounds were then sketched using Marvin Sketch software,[43] and their 3D structures were produced through the program OPEN-BABEL.[44] The compounds were then prepared for docking, utilizing the LigPrep[45] module of Maestro, which filters and desalts ligands based on default criteria and generates possible ionization and tautomeric states for ligands at target pH 7.0 ± 2.0.

Finally, the prepared AurA receptor and compounds (**1**−**5**) were docked through Glide extra-precision docking (Glide XP), a grid-based ligand docking program incorporated in Maestro. Glide XP comprehensively approximates an extensive exploration of the ligand's conformational, orientation, and positional binding pose in the receptor.[46] The resultant docked AurA−compound complexes were then evaluated for their possible binding modes and protein−ligand noncovalent interactions through the Glide XP visualizer. The best-docked pose for each compound was then refined by the steepest descent energy minimization method with default parameters (minimization stops when 75 iterations have been performed or the maximum change in distance between atoms is less than 0.1 Å) to remove any steric clashes. The minimized top docked pose for each compound with AurA was chosen for validation of the binding complexes' structural and interactional stability in an explicit solvent compared to free AurA by molecular dynamics (MD) simulations.

2.2. MD Simulation. MD simulation is a computational technique that simulates the natural motion of a biomolecular system (atoms and molecules) for a predefined period of time to analyze their physical behavior and interactive stability to present a comprehensive view of the dynamic evolution of the system. In this study, MD simulation for a specific time scale (200 ns) was performed to evaluate the dynamic stability of free AurA and each AurA−compound complex employing the DESMOND simulation module.[47] To initialize the MD setup, each system was first prepared using the System builder package included in Desmond. To solvate the systems, the 4-site transferable intermolecular potential (**TIP4P**) water model was utilized, which was defined by setting an orthorhombic box with periodic boundary conditions with edges atleast 10 Å away on all sides from any nearby solute or atoms across the protein structure. The prepared solvated model was first charge neutralized by the addition of counter ions (Na^+ or Cl^-), and then, 0.15 M NaCl ions were added to the system to depict the background salt in physiological conditions. The prepared system was then energy minimized by utilizing 2000 iterations of the hybrid method of the steepest descent and the limited-memory Broyden−Fletcher−Goldfarb−Shanno algorithms to equilibrate and reduce its overall potential energy. The energy-minimized solvated system was further relaxed by utilizing the integrated relaxation protocol in Desmond's "Molecular Dynamics" package. In this protocol, a series of minimizations and short MD simulations are performed in a series of time steps (1−24 ps) with the aid of Brownian dynamics and the Berendsen *NVT* and *NPT* ensemble to raise the temperature of the system gradually from 0 to 300 K, for a total equilibration time of 100 ps.[48−50] The final MD production run was performed for 200 ns with a constant temperature of 300 K, pressure of 1.013 bar with a thermostat, and barostat relaxation times of 1 and 2 ps under the isothermal isobaric ensemble (*NPT*).[51] To maintain a constant temperature and pressure throughout the MD run, the Nosé−Hoover thermostat and the Martyna−Tobias−Klein barostat methods were used.[52−54] The r-RESPA integrator was used to calculate the nonbonded forces, where the short-range forces were updated every 2 fs, and the long-range forces were updated every 6 fs.[55] Further, a 9 Å cut-off radius was set for Coulomb interactions. The simulated system's energy was recorded at a consistent interval of 1.2 ps, while the trajectories were saved at intervals of 200 ps, as required for further analysis. The OPLS4 all-atom force field with default parameters was applied for all the simulation runs. OPLS4 makes for a highly accurate and unwavering molecular mechanics force field that provides a near-credible atomistic simulation of complex biomolecular systems.[56] Further, to compute the long-range inter- and intramolecular electrostatic interactions with the particle mesh, the EWALD geometric algorithm incorporated in DESMOND was implemented.[57,58] The behavior and interactions among each compound and the AurA protein were explored employing the simulation interaction diagram package incorporated in Desmond. The stability of the predicted model system was determined through a comparison of the overall root mean square deviation (RMSD) of the free AurA protein and compound-bound AurA atomic positions in time and their respective trajectories. Furthermore, the protein regions with maximum fluctuation during MD simulations were identified using the protein root-mean-square fluctuation (RMSF) plot. The number and strength of various noncovalent interactions formed between the ligands and protein were calculated through Protein−Ligand Contact plots.

2.3. Molecular Mechanics with Generalized Born and Surface Area Solvation (MM/GBSA) Calculations. The last 500 frames of each MD-refined AurA-compound trajectory were accessed to compute their net molecular mechanics with Generalized Born and surface area solvation (MM/GBSA) binding free energy using the thermal_mmgbsa.py script incorporated in the Schrodinger suite.[59,60]

https://doi.org/10.1021/acsomega.2c00740
ACS Omega 2022, 7, 39603−39618

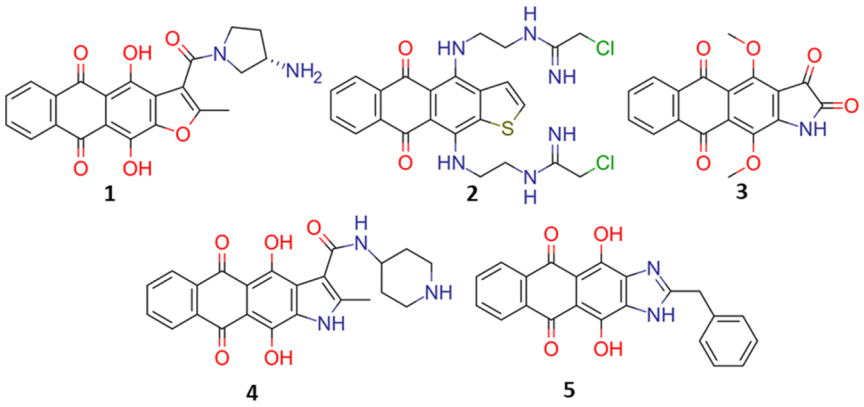

Figure 2. 2D structures of the paternal anthrafuran **1** and its analogues **2**−**5**. Adapted in part from Singh et al.* Heteroarene-fused Anthraquinone derivatives as potential modulators for AurB. DOI: 10.1016/j.biochi.2020.12.024. Copyright 2021. Biochimie.

2.4. Cloning and Expression of Human AurA. The AurA (125−392) gene was isolated from the human leukocyte cDNA library and amplified through a polymerase chain reaction (PCR) applying the forward primer 5-CATGC-CATGGGAAAGAGGCAGTGGGCTTTGG-3 and the reverse primer 5-CCGCTCGAGCTAATTTGATGGTTTT-GATGAATTT-3 containing *Nco1* and *Xho1* restriction sites. These PCR-amplified DNA fragments were ligated to the cloning vector (pET28b) between the *Nco1* and *Xho1* restriction sites, and the clone was confirmed by colony PCR. The AurA gene in pET28b possesses a C-terminal noncleavable $(His)_6$ tag. The pET28b-AurA construct was verified by DNA sequencing. The cloned construct's protein expression was realized in the *E. coli*, Rosetta (DE3) cells at 21 °C for 13−15 h using 0.5 mM IPTG and confirmed by a 12.5 % (w/v) sodium dodecyl sulfate−polyacrylamide gel electrophoresis (SDS−PAGE) run (Figure S1A).

2.5. Purification of Human AurA. For AurA protein purification, the cells were first harvested as cell pellets and subsequently resuspended in a binding buffer comprising 50 mM Tris−HCl (pH 8.0), 300 mM NaCl, 5 mM imidazole, 20 mM $MgCl_2$, 5 mM β-mercaptoethanol (BME), and 10% (vol/vol) glycerol to which ethylenediaminetetraacetic acid-free protease inhibitor cocktail from Roche (Sigma-Aldrich) was additionally supplemented. The cell lysis was achieved utilizing ultrasonication, and the cell lysate was centrifuged for 30 min at 35,000*g* at 4 °C. The processed supernatant was loaded into the NiNTA metal affinity resin (GE Healthcare), previously equilibrated with binding buffer. The affinity purification column was cleaned by 10 column volumes of washing buffer comprising 50 mM Tris−HCl (pH 8.0), 300 mM NaCl, 50 mM imidazole, and 20 mM $MgCl_2$ supplemented with 10% (vol/vol) glycerol and 5 mM BME to eliminate any nonspecifically bound proteins. Finally, the resin-bound AurA was eluted with an elution buffer containing 50 mM Tris−HCl (pH 8.0), 300 mM NaCl, 500 mM imidazole, and 20 mM $MgCl_2$ supplemented with 10% (vol/vol) glycerol and 5 mM BME. All the AurA purification steps were performed at a constant temperature of 4 °C. The homogeneity of purified AurA protein was verified with a 12.5 % (w/v) SDS−PAGE run (Figure S1B). The purified eluted protein was buffer exchanged [50 mM Tris−HCl pH 7.4, 150 mM NaCl, 20 mM $MgCl_2$, 1 mM DTT, and 5% (vol/vol) glycerol] with a PD-10 desalting column and finally concentrated to 5 mg/mL and divided into two batches, with one concurrently utilized for performing planned biophysical experiments and the other flash-frozen with liquid nitrogen and stored at -80 °C refrigeration till further use.

2.6. Synthesis of Compounds. All the synthesized compounds **1**−**5** have been procured through the Gause Institute of New Antibiotics, Russia. Compounds **1**−**3** were chemically synthesized by employing the previously established protocols,[37,61,62] while compounds naphthoindole **4** and anthraimidazole **5** were synthesized according to the new synthetic schemes.[38] The purity of all samples was ≥95%, as confirmed by high-performance liquid chromatography (HPLC) measurements (Figures S2−S6). The 2D chemical structures of all compounds (**1**−**5**) are shown in Figure 2.

2.7. Fluorescence Spectroscopy. Tryptophan quenching studies were used to measure the binding interactions of synthesized compounds (**1**−**5**) with recombinantly purified AurA *in vitro*. Experiments were conducted on a Jasco Spectrofluorometer (FP-6200) with a quartz cuvette of 1 cm path length at pH 7.5 and temperature 25 °C utilizing a thermostat water circulator Peltier device. Working concentrations of compounds were prepared by dissolving them in dimethyl sulfoxide and diluting them in TBST buffer comprising 50 mM Tris, 150 mM NaCl, 1 mM DTT, and 0.01 % Tween 20. A concentration range of 1−200 μM of each synthesized compound **1**−**5** was used for the experiment. After the excitation of tryptophan residues present in AurA (Trp128, Trp277, Trp313, and Trp382) at 280 nm, the resultant emission spectra of AurA in different concentrations of each compound were recorded in the set wavelength range of 300−400 nm. The width of excitation and emission slit for all the experiments was set at 5 nm. For baseline correction, the spectral readings were subtracted from the corresponding blank containing each compound separately in assay buffer without AurA protein. Further, corresponding buffer controls were quantified to check and eliminate any fluorescence intensity signal if produced by the buffer. The experimental findings were evaluated by incorporating the saturation curves data in the SigmaPlot curve fitting wizard's nonlinear eq 1.

$$F = a + (b - a)\cdot((x + 0.5 + K_d) - ((x + 0.5 + K_d)^2 - 2\cdot x)^{0.5}) \quad (1)$$

2.8. Biolayer Interferometry (BLI) Assay. The binding affinity of the compounds **1**−**5** and AurA protein was examined further in real time by biolayer interferometry (BLI) experiments on the Octet-Red96 platform (FortéBio Inc., USA).[63] BLI is a label-free optical analysis technique that

https://doi.org/10.1021/acsomega.2c00740
ACS Omega 2022, 7, 39603−39618

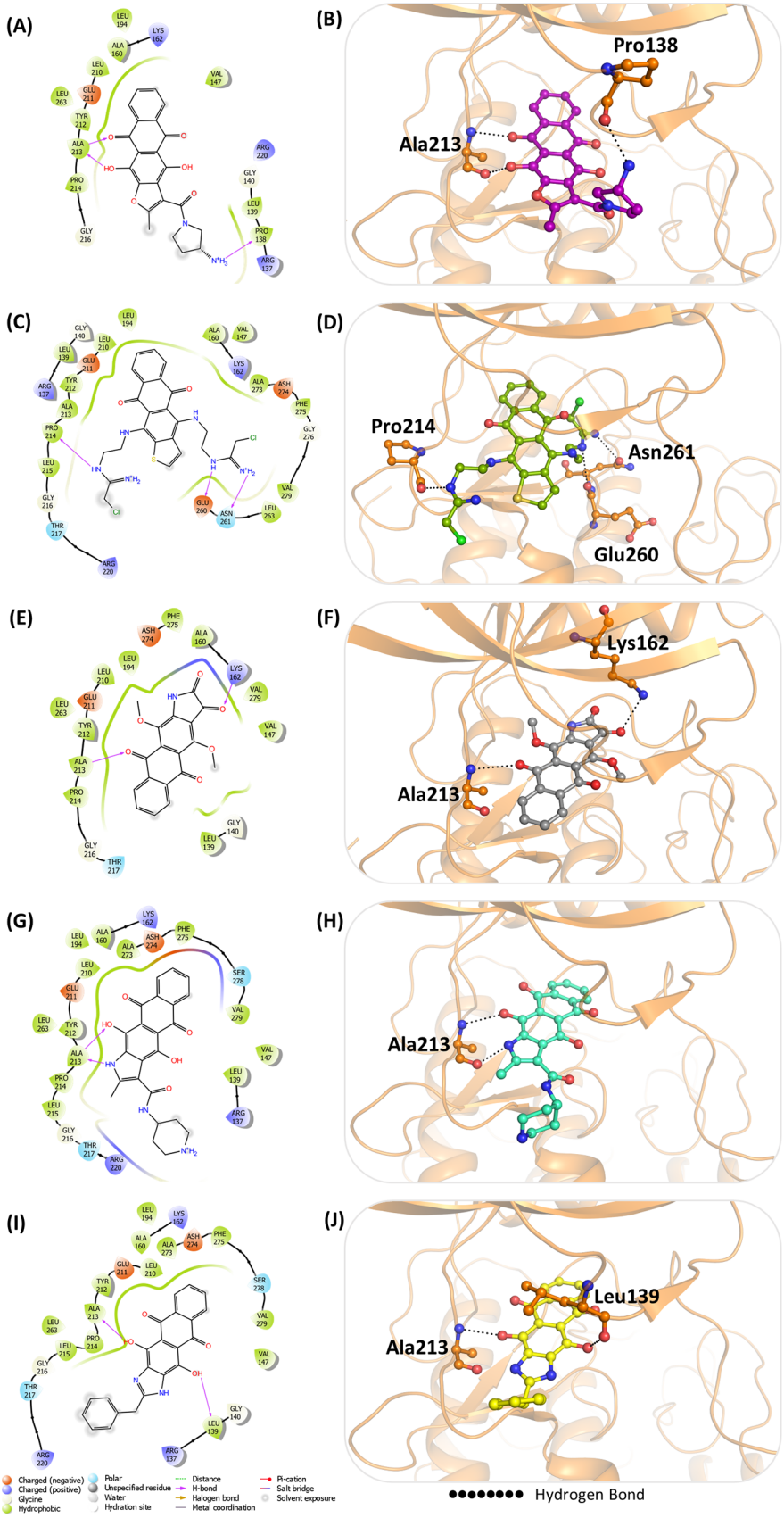

Figure 3. 2D and 3D diagrammatic representation of molecular docking analysis of AurA with compound anthrafuran **1** (A,B), anthrathiophene **2** (C,D), naphthoisatine **3** (E,F), naphthoindole **4** (G,H), and anthraimidazole **5** (I,J).

https://doi.org/10.1021/acsomega.2c00740
ACS Omega 2022, 7, 39603−39618

analyzes the resultant interference pattern of white light reflected from the two surfaces: the biosensor tip with a coating of immobilized protein molecules and an internal reference layer, in real time and solution. To initiate the experiment, C-terminal His-tagged AurA was first loaded on the nickel-charged nitrilotriacetic acid (NTA) sensor tip. Subsequently, the unbound AurA was removed by placing the sensors in HBST assay buffer comprising 25 mM HEPES, pH 7.4, and 200 mM NaCl, supplemented with 0.01 % Tween 20 and 0.1 mg/mL BSA. To commence the association of compounds, AurA-coated NTA sensors were then dipped and incubated with serially diluted concentrations of each compound (**1**−**5**) at 1000 rpm microplate shaking for 180−360 s until peak saturation was seen in separate binding experiments. The corresponding dissociation of the loaded AurA−compound complex was observed by soaking the loaded sensors in the HBST assay buffer. The response data from the biolayer surface were normalized by subjecting a reference NTA sensor without bound AurA concurrently through a procedure similar to that used for the NTA sensors loaded with AurA and subtracting the reference response from the primary response data. This step eliminates the accessory nonspecific binding and buffer-induced interferometry spectrum shift. The experiments were conducted in 96-well Greiner black microwell plates at a steady temperature of 25 °C. The real-time data were analyzed, and the resultant association curves were utilized to calculate the steady state affinity (K_d) values using the in-built Curve fit 1:1 homogenous binding model algorithm for compounds (**1**−**3**) and 2:1 heterogenous binding model algorithm for compounds naphthoindole **4** and anthraimidazole **5** in the Octet Data Analysis package.

3. RESULTS AND DISCUSSION

3.1. Molecular Docking of Compounds with AurA. The ATP binding active site pocket of AurA is majorly a nonpolar site and surrounded by mainly hydrophobic residues Leu139, Val147, Ala160, Leu164, Leu194, Leu210, Tyr212, Ala213, Pro214, Leu210 Leu215, Leu263, Ala273, Phe275, and Val279. The core of all the five compounds has a linear heteroarene-fused anthraquinone scaffold, which is a plane nonpolar aromatic system that can comfortably fit into the hydrophobic binding pocket of AurA. The observed binding mode mechanism of the core heterocyclic scaffold is comparable in position (near the hinge region of the active site) for all the compounds (**1**−**5**) with highly similar orientation in naphthoindole **4** and anthraimidazole **5**, differing marginally in anthrafuran **1**. The orientation of anthrathiophene **2** having the bulky 4,11-bis(2-(chloroacetamidino)-ethylamino) substituent moieties attached to the central core of the compound orient themselves toward a suitable space to further increase the interactions with AurA atoms. Interestingly, though the position of naphthoisatine **3** in the binding pocket closely resembled that of naphthoindole **4** and anthraimidazole **5**, its orientation was observed to be flipped by a complete 180°, which positioned its terminal pyrrole-2,3-dione moiety in the vicinity of the flexible region and activation loop residues.

The analysis of the protein−ligand interactions after docking indicated that anthrafuran **1** occupied the ATP-binding cleft. The stabilization of the complex was mainly due to nonpolar interactions with hydrophobic residues of amino acids (Figure 3A). This was further stabilized through hydrogen bonds involving the oxygen and hydroxyl atoms of the quinoid fragment with the carbonyl and amino group of the Ala213 hinge region residue. The amino group of the terminal pyrrolidine moiety also formed additional hydrogen-bonding interaction with the sidechain carbonyl oxygen of Pro138 (Figure 3B). Subsequently, the docking of derivative compounds **2**−**5** in the corresponding AurA site was carried out.

Anthrathiophene **2** has the largest substituent moieties among the five derivatives. Its core scaffold reorients itself to accommodate these 4,11-bis(2-(chloroacetamidino)-ethylamino) moieties comfortably inside the binding pocket. Three of the six potential hydrogen bond donor atoms (amino- and imino-groups) of the 4,11-bis(2-(chloroacetamidino)-ethylamino) arms formed hydrogen-bonded interactions with sidechain oxygen atoms of hinge region residue of Pro214 and front loop residues of Glu260 and Asn261 (Figure 3C,D). The hydrophobic core of compound **2** was surrounded by the sidechains of hydrophobic, polar, and charged active site residues enabling it to form additional stabilizing noncovalent interactions within the active site (Figure 3C).

The character of the binding of naphthoisatine **3** in the ATP binding active site of AurA is similar to that of the pyrazole-benzimidazole-based inhibitors, for example, PHA-680632, which also binds at this site.[64] The 180° degree inversion of naphthoisatine **3** while on one side positioned its quinoid oxygen in the vicinity of the amino group of the hinge region residue, Ala213, enabling a single hydrogen-bonding interaction; it additionally rearranged the positioning of its terminal pyrrole-2,3-dione moiety in the vicinity of the flexible region and activation loop residues enabling its 3-carbonyl oxygen atom to form additional stable hydrogen bonding interaction with Lys162 (Figure 3F). The complex was further stabilized through numerous noncovalent interactions with the sidechains of hydrophobic, polar, and charged active site residues of AurA, including that with the sidechain of polar catalytic triad residues Thr217 (Figure 3E).

The predicted orientation of naphthoindole **4** and anthraimidazole **5** is reasonably similar, wherein their polyannelated core overlaps almost entirely. However, the observed slightly different orientation enables anthraimidazole **5** to develop additional hydrogen-bond interactions with the sidechain of Leu139. The hydroxyl groups of the polyannelated core of naphthoindole **4** and anthraimidazole **5** were observed to form similar hydrogen-bond interactions with the amino group of Ala213, while the pyrrolidine amino group of naphthoindole **4** interacts additionally with the carbonyl group of Ala213. (Figure 3H,J). Similar to the other compounds, the hydrophobic cores of naphthoindole **4** and anthraimidazole **5** were involved in several hydrophobic, charged, and polar interactions including those with the catalytic triad residues Leu215, Thr217, and Arg220, additionally stabilizing the complex inside the active site binding pocket (Figure 3G,I). All noncovalent bonding interactions of compounds (**1**−**5**) observed inside 4 Å with AurA are listed in Table S1.

3.2. Structural Changes in AurA upon Compound Binding. The docking computations were followed by MD simulation studies to assess the stability and flexibility behavior of the free AurA structure and the docked complexes. MD simulations have become a widely used approach to not only gain valuable acumen into the structural dynamics and functional process of protein−ligand bound complex but also to illustrate the dynamics of the ligand's binding prototype with the protein in the explicit solvent medium.[65,66] Here, an

https://doi.org/10.1021/acsomega.2c00740
ACS Omega 2022, 7, 39603−39618

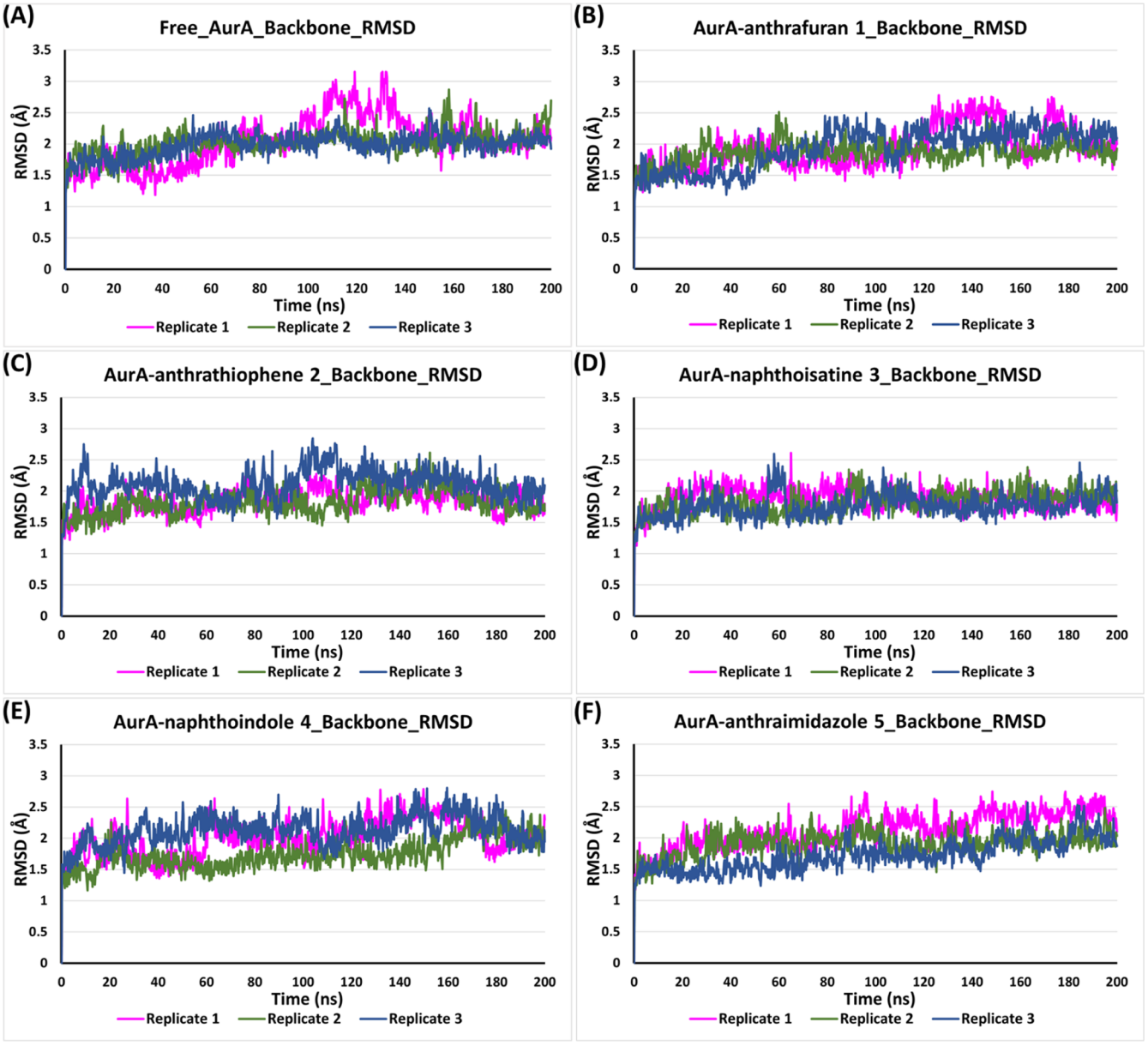

Figure 4. MD simulation trajectory analysis of free AurA and AurA−compound complexes. RMSD fluctuation plots for the backbone atoms of (A) free AurA, (B) AurA−anthrafuran **1**, (C) AurA−anthrathiophene **2**, (D) AurA−naphthoisatine **3**, (E) AurA−naphthoindole **4**, and (F) AurA−anthraimidazole **5**.

all-atom MD simulation study of AurA in the free state and compound-bound complex state was done for 200 ns in triplicates to elucidate the conformational dynamics, complex steadiness, and mechanism of interactions of each compound with AurA. Upon binding in the active site, a ligand molecule can result in large conformational changes in a receptor's structure. Hence, the calculation of RMSD forms an effective approach to monitor the structural stability and conformational deviations in a protein. To corroborate the conformational and structural stability of the AurA backbone before and after binding with each compound, the resultant RMSD of the simulated systems were recorded and analyzed (Figure 4A−F).

From the RMSD plot, we inferred that all the docked complexes, except naphthoindole **4**, displayed a reasonably stable trajectory during the simulation time of 200 ns. The simulation trajectories of the naphthoindole **4**-docked complex were observed to follow a slightly more flexible behavior in all of the simulation replicates with higher fluctuations (Figure 4E) with its corresponding heavy atoms trajectories also stabilizing at a higher average RMSD value of ∼4 Å (Figure S7D). The observed RMSD of the free AurA protein backbone atoms demonstrated a stable behavior between 1 and 2.5 Å in two of the three replicates, except one replicate, where the resultant trajectory showed higher flexibility and increased fluctuations during the entire simulation time (Figure 4A). For the AurA-anthrafuran **1** dock complex, the RMSD trajectories were also found to be within 2.5 Å for the majority of simulation time in all the replicates (Figure 4B). The corresponding heavy atoms trajectories of anthrafuran **1** were also quite stable with minor fluctuations indicating a stable binding mode in the active site (Figure S7A). In two of the three anthrathiophene **2** docked complex simulation replicates, AurA backbone atoms and corresponding anthrathiophene **2** heavy atoms showed similar stable fluctuation behavior, except

https://doi.org/10.1021/acsomega.2c00740
ACS Omega 2022, 7, 39603−39618

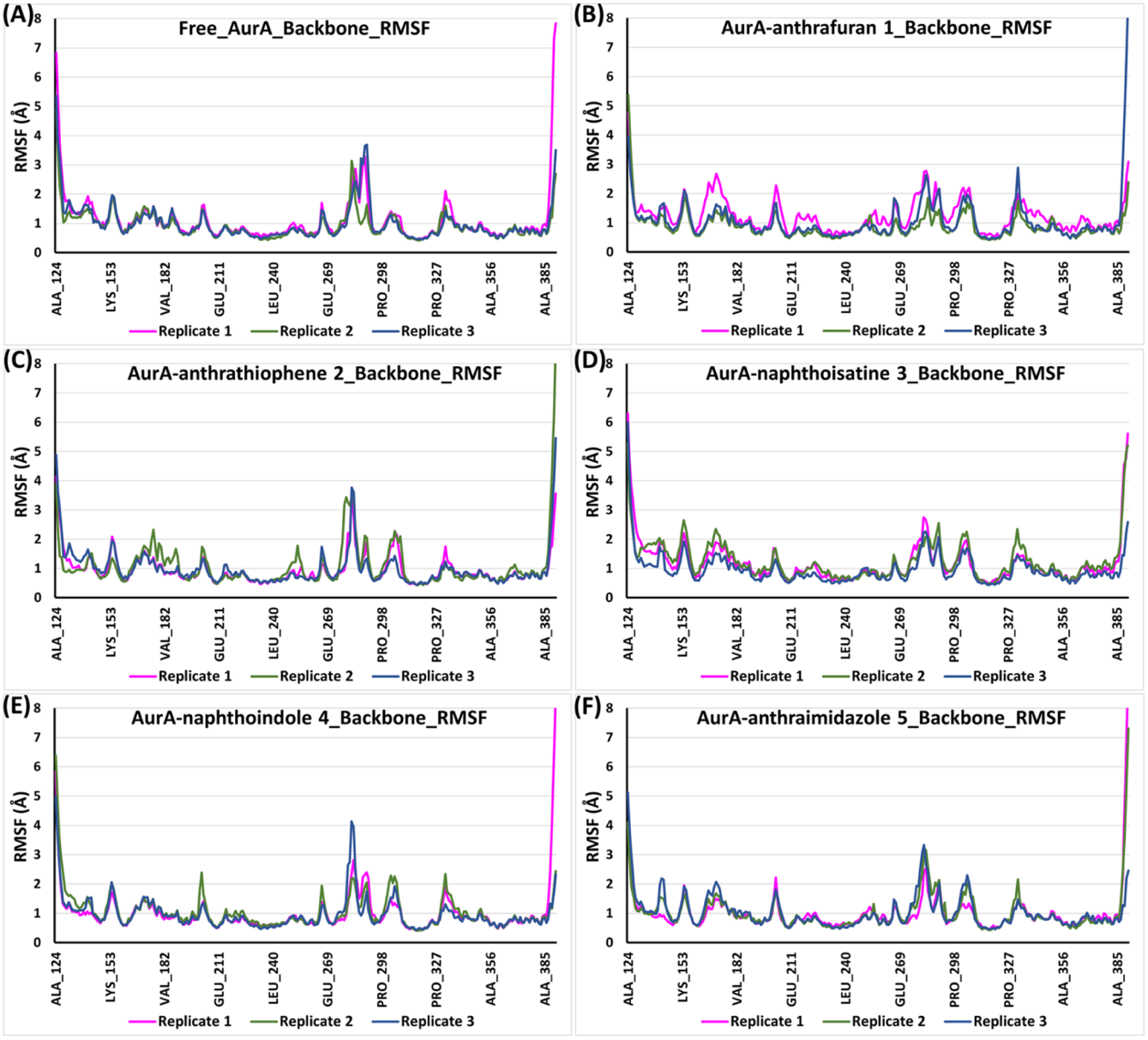

Figure 5. MD simulation RMSF analysis of free AurA and AurA−compound complexes amino acid residues. RMSF fluctuations plots for backbone atoms of (A) free AurA, (B) AurA−anthrafuran **1**, (C) AurA−anthrathiophene **2**, (D) AurA−naphthoisatine **3**, (E) AurA−naphthoindole **4**, and (F) AurA−anthraimidazole **5**.

replicate 3, where they followed slightly flexible trajectories (Figure 4C) (Figure S7B). The simulation replicates of the naphthoisatine **3**-docked complex indicated that the AurA backbone atoms followed very stable trajectories with an average RMSD of ∼2 Å, and the least fluctuation behavior complemented equally well with naphthoisatine **3** heavy atom trajectories that incurred acceptable fluctuations with an average of < 2.5 Å (Figure 4D) (Figure S7C). This warrants the presence of the stabilizing effect of naphthoisatine **3** on the global dynamics of the AurA structure, leading to less conformational changes compared to its free conformation. The docked complex trajectories of anthraimidazole 5 (Figure 4F) were observed to propagate with minor fluctuations within 2.5 Å, with its corresponding heavy atom trajectory following a very similar path and stable fluctuation behavior (Figure S7E). Overall, after comparing the dock complexes' RMSD behavior with free AurA trajectories, the findings indicate that the binding of each compound in the AurA active site induced acceptable fluctuation behavior within the 1−3 Å range, with a mean value of <2.5 Å after the 200 ns simulation time scale.

Further, the structural flexibility of the AurA backbone was checked utilizing the RMSFs value to evaluate the average residual fluctuations of each residue before and after binding of the compounds. A high RMSF value indicates higher per residue fluctuations in protein, while a low value portrays stable orientation. From the RMSF plot, it was inferred that all the systems sported a relatively similar fluctuation behavior with average RMSF values of <3 Å (Figure 5A−F). The amino acid residues comprising the N- and C-terminals displayed a higher degree of fluctuations for all the docked complexes, similar to the free AurA. A corresponding decrease in the fluctuations span was observed in the region comprising the activation loop (residues 274−299) for compound anthrafuran **1** and naphthoisatine **3**, indicating formation of stabilizing

https://doi.org/10.1021/acsomega.2c00740
ACS Omega 2022, 7, 39603−39618

interactions with the residues in the region (Figure 5D). Similarly to the free AurA, the average RMSF of the residues surrounding the AurA active site, including the hinge region containing the catalytic triad residues (Leu215, Thr217, and Ar220), were observed to be maintained with minimal fluctuations, indicating minimal conformational impact and sturdy binding of the compounds with the AurA residues in the region. Overall, the RMSF plots reflected that the fluctuation behavior of AurA residues was not majorly impacted upon binding of the compounds with naphthoisatine **3**, providing a further decrease in residual fluctuations in the activation loop region.

3.2.1. Interaction Analysis of the AurA−Compound Complex. The formation of hydrogen bonds within the protein structure is a foundational characteristic of its conformational stability. Probing the hydrogen-bonding interactions between a ligand and a receptor can provide extensive insight into not only the stability of the complex but also provides relevant information on the directionality and specificity of receptor−ligand interactions. The post-MD interaction analysis of the AurA−anthrafuran **1** complex revealed that the complex stability was majorly supported by hydrogen-bonding interactions with hinge region residue Ala213 and Leu139 and water-mediated interactions with catalytic residue Thr217, which were observed to be maintained for a minimum of 50% of simulation time in all the replicates (Figure S8A). The quinone moiety in the anthraquinone core of all the docked compounds (**1**−**5**) was observed to interact with the hinge region residue Ala213 via hydrogen bonds for the majority of the simulation time, which reaffirms the specific interaction's importance in the fixation of small molecules in the active site and their corresponding contribution to good binding affinity with AurA.[25,27,67] The loss of this specific interaction has been observed to lead to a loss of affinity of potential inhibitors with AurA.[68] The large 4,11-bis(2-(chloroacetamidino)ethylamino) moieties of anthrathiophene **2** provided its further flexibility in the active site binding pocket of AurA. This enabled it to form additional stabilizing hydrogen bonding interactions with the hinge region residue Pro214 through its 4-((2-chloroacetamidino)-ethylamino) arm in all the three MD replicates and water-mediated hydrogen bonding interactions within the vicinity of the activation loop region with residues Glu260 and Asp274 via its 11-((2-chloroacetamidino)ethylamino) arm in one of the replicates (Figure S8B). The presence of terminal pyrrole-2,3-dione ring in naphthoisatine **3** facilitates it to form additional stable hydrogen bonding and water-mediated interactions in the vicinity of phosphate-binding and activation loop regions with residues Lys162 and Asp274 in all the three replicates and with Lys141 and His280 in one MD replicate (Figure S8C). Studies have indicated that compared with an R group in the solvent-accessible region, the orientation of the R1 group in the phosphate-binding region always leads to stronger interactions with AurA kinase,[25] which can be attributed to the enhanced binding mode of naphthoisatine **3** in the AurA active site. Additionally, the primary benzene ring of naphthoisatine **3** further stabilized the complex in the active site by forming stable hydrophobic contacts with Tyr212 and Leu139 residues (Figure S8C). The interaction profile of naphthoindole **4** and anthraimidazole **5** in the active site is quite similar, with their primary benzene ring forming hydrophobic contacts with Ala160 and Leu263 residues. Additionally, the terminal pyrrole nitrogen in both naphthoindole **4** and anthraimidazole **5** interacts with hinge region residues of Tyr212 and Pro214 via water-mediated hydrogen bonds (Figure S9A,B). The improved binding mode in the case of anthraimidazole **5** compared to naphthoindole **4** can be attributed to its 4-OH additional hydrogen bonding interaction with the side chain amino group of Ala213.

3.2.2. Binding Free Energy Calculations (Prime MM/GBSA). The value of ΔG_{bind} is suggestive of the binding affinity between the receptor and ligand complex, where a more negative value represents a stronger binding between them.[69] The MM/GBSA calculations for each AurA−compound docked complex were performed for computing their binding free energies by incorporating the last 500 frames of each complex's simulation trajectory. The resultant calculations confirmed the findings of the docking and MD simulations that all the compounds (**1**−**5**) bind in the AurA active site with a decent binding affinity (Table S2). The net binding free energy computation comprised contributions from covalent, coulomb, hydrogen bonding, van der Waals, lipophilic, and polar solvation energy. Among them, the most substantial contributors were found to be van der Waals and Coulomb energy, while the smallest contributions were obtained through polar solvation energy (Table S2). Higher negative values of van der Waals energy implies that the molecules were involved in strong interactions with the proteins.[20] The average contributions of coulomb interaction energy were found to be higher for AurA−naphthoisatine **3** complexes as compared to other compound complexes, with anthrathiophene **2** scoring the lowest (Table S2). The lowest MM/GBSA binding free energy (ΔG_{bind}) was recorded for the naphthoisatine **3**-docked complex that largely correlates with the MD simulation results, which highlighted its stabilizing effect on the AurA structure, highly stable binding mode with minimum fluctuations, and a stable similar set of interactions including direct hydrogen bonding interactions with Ala213 and Lys162 and water-mediated hydrogen bonding interaction with Asp274, additionally supported by hydrophobic contacts with Leu139 and Tyr212.

3.3. *In Vitro* Binding of Compounds with Purified AurA. *3.3.1. Fluorescence Spectroscopy.* Fluorescence-based techniques are extensively used to study not only the chemical environments but also the intermolecular interactions of ligands with the target receptors. If a suitable change in fluorescence is detected upon binding of the ligand to the receptor, it can be observed to gather evidence on both the properties of the equilibrium complex and the associated kinetics of interaction, that is, the conformational fluctuations that help in attaining the equilibrium state. Fluorescence quenching in biomacromolecules can be attained through a number of interactions, including a ground−state complex arrangement among the quencher and fluorophore, excitation of charge−transfer complex, intersystem cross-over toward triplet state, and molecular reorganizations.[70−73]

Hence, to examine the *in vitro* binding affinity of heteroanthraquinone compounds **1**−**5** with AurA, tryptophan (Trp) quenching-based fluorescence emission was used as a probe. AurA has four Trp-residues (Trp128, Trp277, Trp313, and Trp382) that can act as ideal fluorophores and thus can be utilized for the ligand-binding experiments applying the fluorescence quenching technique. In response to ligand binding, a desired shift in emission spectra of Trp residues of AurA was detected, as it altered the environment bordering the indole ring of a Trp-residue in a distance-relative mode.

https://doi.org/10.1021/acsomega.2c00740
ACS Omega 2022, 7, 39603−39618

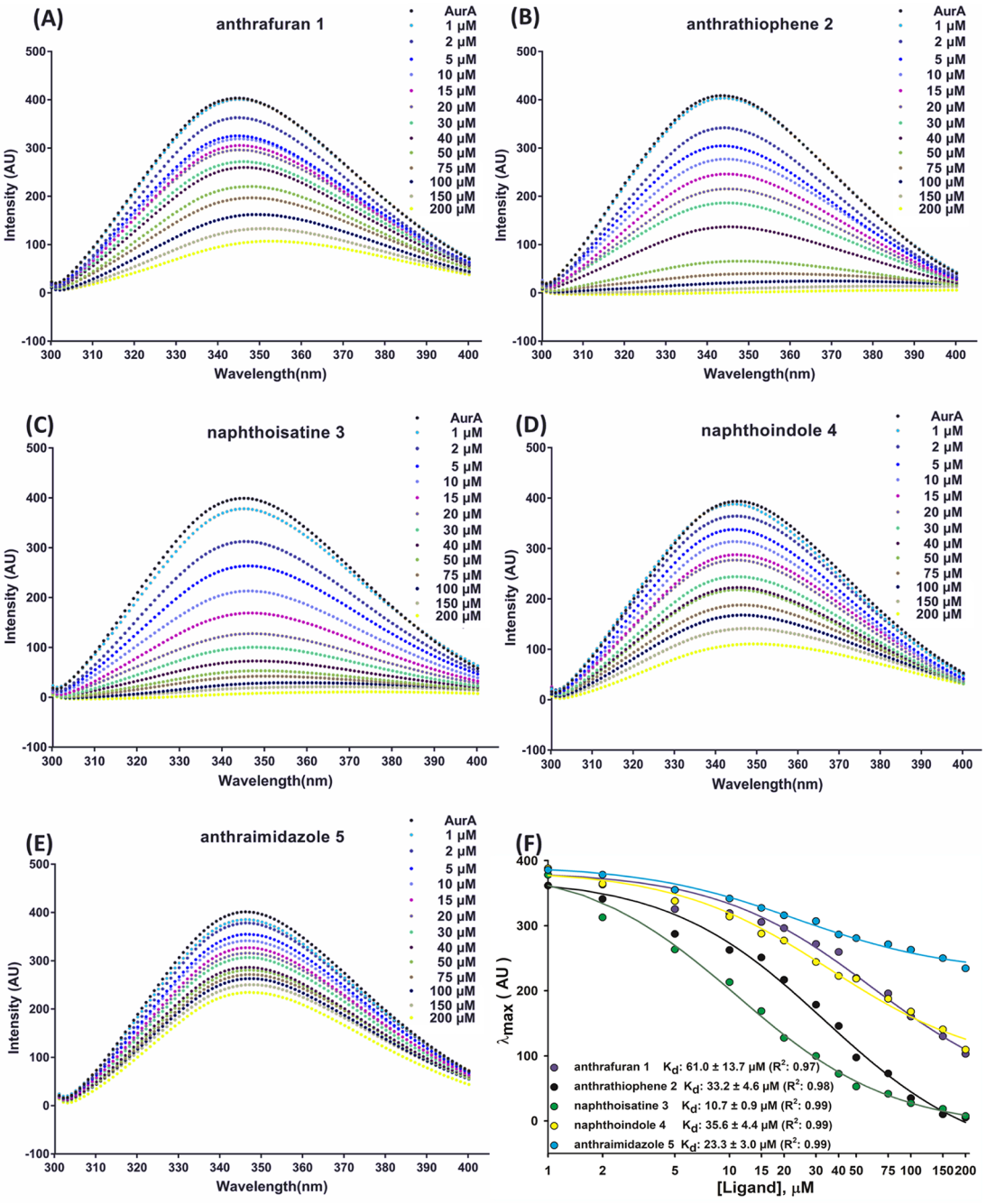

Figure 6. Intrinsic fluorescence binding studies of synthesized compounds (A) anthrafuran **1**, (B) anthrathiophene **2**, (C) naphthoisatine **3**, (D) naphthoindole **4**, and (E) anthraimidazole **5** with AurA. After excitation of tryptophan (Trp128, Trp277, Trp313, and Trp382) residues at 280 nm, the resultant emission spectra of AurA (3.0 μM) in increasing concentrations of compounds (0−200 μM) were noted in the wavelength scale of 300−400 nm. (F) Fluorescence intensity values were recorded at 342 nm and subsequently mapped as a function of concentrations of compounds on a logarithmic scale to calculate the binding affinity parameters.

The binding ability of the compounds with AurA was studied in the concentration span of 1−200 μM. The maximum Trp-fluorescence of AurA with ligands occurred between 342 and 345 nm. The recorded emission spectra of AurA's intrinsic fluorescence with increasing concentrations of each compound are shown in Figure 6A−E.

The discrete binding of each compound with AurA produced a hypsochromic shift or blue shift of 2−3 nm emission maxima toward a lesser wavelength. Additionally, this diminished the Trp fluorescence intensity in a compound concentration-dependent mode, indicating the shift in polarity of the Trp residues from polar to nonpolar or a more buried environment. Naphthoisatine **3** and anthrathiophene **2** showed a considerable decrease in Trp fluorescence with every dilution. The maximal recorded fluorescence intensity at 342 nm (λ_{max}) for AurA against varying concentrations of each compound was mapped to produce saturation curves. The K_d value for all compounds was subsequently determined from the nonlinear, single-site saturation model for all baseline (Figure S10B) corrected recorded curves (Figure 6F). Among all the synthesized compounds (**1**−**5**), naphthoisatine **3** (K_d 10.7 ± 0.9 μM) and anthraimidazole **5** (K_d 23.3 ± 3.0 μM) were

https://doi.org/10.1021/acsomega.2c00740
ACS Omega 2022, 7, 39603−39618

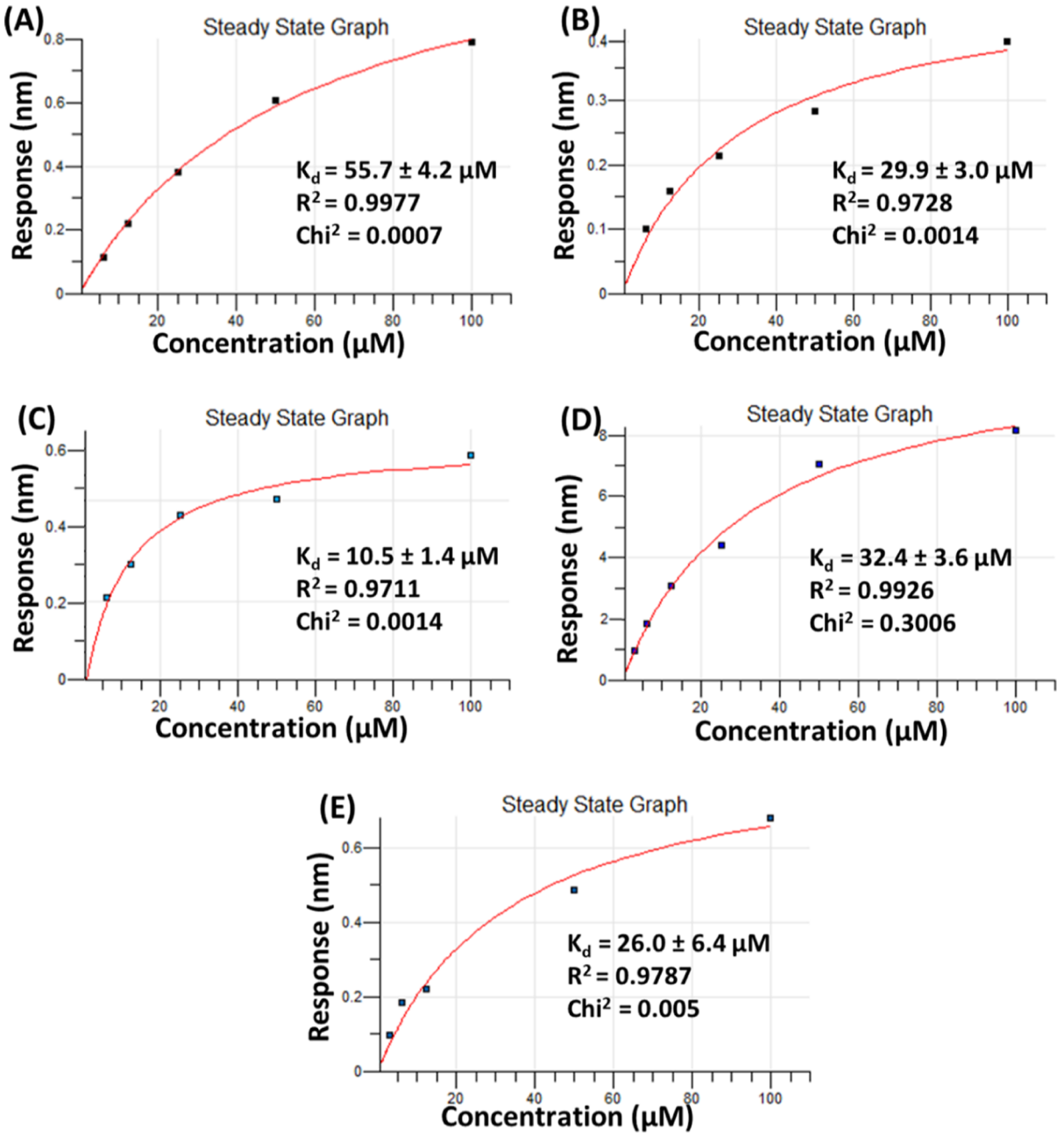

Figure 7. Steady state binding affinity analysis of AurA-complexes through the BLI assay. The obtained association curves for each concentration of compounds with AurA were fitted onto a 1:1 binding model for compounds (**1**−**3**) and a 2:1 heterogenous binding model for compounds **4** and **5**. The resulting fitting plots for (A) anthrafuran **1**, (B) anthrathiophene **2**, (C) naphthoisatine **3**, (D) naphthoindole **4**, and (E) anthraimidazole **5** are shown above.

revealed to possess an enhanced binding affinity with AurA followed by anthrathiophene **2** (K_d 33.2 ± 4.6 μM) and naphthoindole **4** (K_d 35.6 ± 4.4 μM), with paternal anthrafuran **1** (K_d 61.0 ± 13.7 μM) showing the least binding affinity.

*3.3.2. Assessment of the Affinity and Specificity of the Synthesized Compounds (**1**−**5**).* The real-time binding kinetics for synthesized compounds was performed by the BLI assay with purified AurA. The resultant data was fitted to obtain steady-state affinity (K_d) values for each compound (**1**−**5**), and it was compared with the steady-state affinity (K_d) results obtained through fluorescence spectroscopy data to further warrant the binding profile of each compound. The binding of each compound (**1**−**5**) in serially diluted concentrations with the immobilized AurA on the surface of the NTA biosensor increased the thickness of the sensor. This was accredited by a subsequent shift in the wavelength interference pattern of the sensorgram in real time. A considerable shift (0−8 nm) in the association curves upon adding different concentrations of each compound (**1**−**5**) to AurA in a concentration-dependent manner was observed (Figure S11). The real-time binding curves (Figures S12 and S13) were calculated by fitting the reference subtracted association curve data globally to a 1:1 binding model for compounds (**1**−**3**) with the equilibrium dissociation constants (K_d) calculations for all protein−ligand complexes. For

https://doi.org/10.1021/acsomega.2c00740
ACS Omega 2022, 7, 39603−39618

compounds naphthoindole **4** and anthraimidazole **5**, the association data curves were found to fit precisely with the 2:1 heterogenous binding model, indicating possible sequential binding of these compounds with the allosteric site of AurA. Though the majority of inhibitors are designed to specifically target only the conserved prominent ATP binding site of AurA, the conformational transitions in AurA structure induced upon ligand binding in the AurA active site may enable the potential inhibitors to additionally access and bind to allosteric sites within the AurA.[25,74,75]

Interestingly, validating the results of *in silico* and fluorescence binding studies, a reasonable interaction *in vitro* between AurA and naphthoisatine **3**, anthraimidazole **5**, and anthrathiophene **2** was seen with K_d values of 10.5 ± 1.4, 26.0 ± 6.4, and 29.9 ± 3.0 μM, respectively. The compound naphthoindole **4** exhibited a K_d value of 32.4 ± 3.6 μM, and while corroborating the previous findings, the least binding affinity was seen in anthrafuran **1**, with a K_d value of 55.7 ± 4.2 μM. The obtained binding curves for AurA and heteroarene-fused anthraquinone derivatives are presented in Figure 7A−E.

3.3.3. Binding Profile of Compounds. Based on the findings of previous studies, potential Aurora kinase inhibitors can be majorly divided into four types. Type 1 inhibitors or ATP-competitive inhibitors, for example, VX680, MLN8054, ML8237, and PHA-680632; type 2 inhibitors, for example, imatinib; type 3 inhibitors or allosteric inhibitors, for example, AurkinA; and type 4 inhibitors also referred to as covalent and reversible inhibitors, for example, coenzyme A.[24,27,28,30,76−79] Our designed compounds closely resemble the type 1 or ATP-competitive inhibitors in the basic chemical structure and features. Type 1 inhibitors typically consist of a heterocyclic core system that occupies and interacts with the hinge region of Aurora kinase and extended sidechains that occupy hydrophobic pockets nearby. For the heterocyclic core scaffold of the compounds, we have utilized the anthraquinone core, which is becoming a highly sought-after scaffold to develop specific and effective novel antitumor therapies,[80] while various modifications at the 4,11 hydroxyl groups position of the anthraquinone core and terminal heterocyclic are aimed to offer further stabilization to the binding mode by contacts of compounds with the hydrophobic back pocket, activation loop, and ATP phosphate binding region of the Aurora kinases' active site.

In the study, similar to the binding mode and the character of known AurA inhibitors (VX680, MLN8054, ML8237, and PHA-680632),[27,28,64,67,81−83] the linear heteroarene-fused anthraquinone core of all the five compounds fit comfortably inside the AurA active site, forming essential polar contacts with hinge and solvent-exposed region residues to fix them in position. Various modifications at the 4,11-hydroxyl group position of the anthraquinone core and the terminal heterocyclic ring further stabilized the binding contacts of compounds (**1**−**5**) with the nearby hydrophobic back pocket, activation loop, and ATP phosphate binding region of the AurA active site, with different modifications providing distinctive interactional profiles.

These findings along with the binding energies of compounds (**1**−**5**) were further corroborated and correlated with the obtained results from BLI and fluorescence quenching experiments (Table 1).

Reiterating the findings of *in silico* studies, naphthoisatine **3** presents itself as the overall best binder in fluorescence quenching and BLI binding assays as well. The results of other tested compounds are also in good agreement with all the modeling and experimental data. As previously tested with AurB,[38] the overall binding mode of compounds anthrafuran **1**, naphthoindole **4**, and anthraimidazole **5** is fairly comparable, except anthrathiophene **2**. While the binding orientation of anthrathiophene **2** is only slightly modified in AurA due to the large horizontal binding pocket which accommodates both 4,11-bis(2-(chloroacetamidino)ethylamino) substituents in the AurA active site (Figure S14), the short vertical binding site of AurB enables anthrathiophene **2** to reorient its structure to accommodate one of its arms in an anchor fit type position deep inside the binding pocket, while the core anthraquinone moiety and its other arm orient toward the solvent-exposed region, allowing it to make additional stabilizing interactions. This orientation of anthrathiophene **2** also potentially acts as a steric barrier to ward off the binding of ATP and other cofactors competitively, as confirmed with AMP−PMP competitive binding experiments with AurB.[38] All these factors greatly influence the binding and inhibition ability of anthrathiophene **2**, presenting it as the better inhibitor candidate in the case of AurB. In the case of AurA, the basic binding profile of all compounds (**1**−**5**) is similar in terms of primary interactions with the hinge region residues in the AurA active site, particularly the hydrogen bonding interactions with Ala213. The structural modifications in the core heteroarene-fused anthraquinone scaffold, specifically the modification of the terminal furan ring of anthrafuran **1** to pyrrole-2,3-dione in naphthoisatine **3**, facilitate the formation of additional stable hydrogen-bonded and water-mediated interactions with the nearby active site residues, particularly in the vicinity of phosphate-binding and activation loop region residues, Lys162 and Asp274. These changes in the scaffold enhance its overall binding strength with AurA. The *in silico* observations are complemented by the biophysical binding assay results. Thus, naphthoisatine **3** presents itself as a prominent binder of AurA among other tested compounds.

Table 1. *In silico* and *In Vitro* Binding Profiles of Compounds 1−5 with AurA

compounds	MMGBSA ΔG binding energy (kcal/mol)	BLI (K_d, μM)	fluorescence spectroscopy (K_d, μM)
anthrafuran 1	−40.0 ± 3.8	55.7 ± 4.2	61.0 ± 13.7
anthrathiophene 2	−46.6 ± 5.2	29.9 ± 3.0	33.2 ± 4.6
naphthoisatine 3	−47.1 ± 4.1	10.5 ± 1.4	10.7 ± 0.9
naphthoindole 4	−41.9 ± 2.1	32.4 ± 3.6	35.6 ± 4.4
anthraimidazole 5	−42.6 ± 1.6	26.0 ± 6.4	23.3 ± 3.0

4. CONCLUSIONS

The current study investigated the binding ability of heterocyclic derivatives of anthraquinone previously found to inhibit AurB, against another important member of the kinase family, viz., AurA protein, through a blend of computational and biophysical methods.

Molecular docking computations revealed that all the compounds (**1**−**5**) bind at the active site of AurA, forming non-covalent hydrogen bonding interactions and hydrophobic contacts with active site residues. A study of conformational dynamics of docked complexes in an explicit solvent environment revealed that they follow relatively stable trajectories with acceptable fluctuations. Docked complexes of naphthoisatine **3** were observed to enhance the conforma-

https://doi.org/10.1021/acsomega.2c00740
ACS Omega 2022, 7, 39603−39618

tional stability and reduce the number of fluctuations in the AurA trajectory, as compared to free AurA.

To test the *in vitro* binding affinity of compounds with AurA and correlate the findings of *in silico* studies, fluorescence quenching studies were undertaken. The observations from the fluorescence spectroscopy binding experiments were further validated with the real-time label-free binding technique of BLI. Compounds naphthoisatine **3** and anthraimidazole **5** were found to be prominent binders of AurA with good binding affinity and saturation property. In conclusion, all the studies indicate that, among the tested compounds, naphthoisatine **3** proves to be the best binder with AurA, followed closely by anthraimidazole **5** and anthrathiophene **2**. Hence, these compounds can be actively pursued to target Aurora kinases as an effective strategy to develop novel drugs for the treatment of the clinical anomalies of cancer related to differential expression of Aurora kinases. In conclusion, our results encourage the use of heteroarene-fused anthraquinone scaffolds for the effective design and development of anticancer agents.

■ ASSOCIATED CONTENT

Supporting Information

The Supporting Information is available free of charge at https://pubs.acs.org/doi/10.1021/acsomega.2c00740.

> AurA expression and SDS gel purification, HPLC data for compounds (**1**−**5**), AurA−compounds' docking interactions data, ligand rmsd plots and the interaction profile of AurA-compounds (**1**−**5**) simulation replicates, additional fluorescence spectroscopy data, BLI raw data for whole experiments and each compound, and AurA-compounds (**1**−**5**) docked superimposed figure (PDF)

■ AUTHOR INFORMATION

Corresponding Author

Punit Kaur − *Department of Biophysics, All India Institute of Medical Sciences, New Delhi, Delhi 110029, India;* orcid.org/0000-0002-7358-3716; Phone: +91-11-2659 4288; Email: punitkaur@aiims.edu, punitkaur1@hotmail.com; Fax: +91-11-2658 8663

Authors

Mandeep Singh − *Department of Biophysics, All India Institute of Medical Sciences, New Delhi, Delhi 110029, India*

Md. Anzarul Haque − *Department of Biophysics, All India Institute of Medical Sciences, New Delhi, Delhi 110029, India;* Present Address: Department of Cellular and Molecular Biology, University of Texas Health Science Center, Tyler, TX, USA. Phone: +1 (903) 787-6197

Alexander S. Tikhomirov − *Gause Institute of New Antibiotics, Moscow 119021, Russia;* orcid.org/0000-0002-6418-1539

Andrey E. Shchekotikhin − *Gause Institute of New Antibiotics, Moscow 119021, Russia;* orcid.org/0000-0002-6595-0811

Uddipan Das − *Department of Biophysics, All India Institute of Medical Sciences, New Delhi, Delhi 110029, India*

Complete contact information is available at: https://pubs.acs.org/10.1021/acsomega.2c00740

Author Contributions

P.K. conceptualized the research. A.S.T. and A.E.S. designed and synthesized the compounds. M.S. designed the workflow; performed the computational studies; cloned, expressed, and purified AurA for biophysical assays; and completed the BLI and fluorescence binding experiments. M.A.H. supervised the fluorescence quenching experiments. U.D. conceived and supervised the cloning and expression experiments. M.S. evaluated the raw data and wrote the manuscript. M.A.H. and P.K. edited and amended the manuscript. The manuscript was thoroughly revised and approved by all authors.

Notes

The authors declare no competing financial interest.

The dataset used in this study is available from Punit Kaur on request.

■ ACKNOWLEDGMENTS

This Indian-Russian joint collaborative research project was funded by the Department of Science and Technology, India (Int/Rus/RFBR/P-291), and the Russian Foundation for Basic Research, Russia (19-33-90179). We are grateful to Dr. Ravi Pratap Singh (Field Application Scientist, Sartorius AG) for his assistance in analyzing BLI experiments.

■ ABBREVIATIONS

AurA, human Aurora kinase A; MD, molecular dynamics; BLI, biolayer interferometry; ITC, isothermal calorimetry; AurB, human Aurora kinase B; AurC, human Aurora kinase C; RMSD, root-mean-square deviation; RMSF, root-mean-square fluctuation; PCR, polymerase chain reaction; BME, β-mercaptoethanol; NTA, nitrilotriacetic acid

■ REFERENCES

(1) Willems, E.; Dedobbeleer, M.; Digregorio, M.; Lombard, A.; Lumapat, P. N.; Rogister, B. The Functional Diversity of Aurora Kinases: A Comprehensive Review. *Cell Div.* **2018**, *13*, 7.

(2) Andrews, P. D.; Knatko, E.; Moore, W. J.; Swedlow, J. R. Mitotic Mechanics: The Auroras Come into View. *Curr. Opin. Cell Biol.* **2003**, *15*, 672−683.

(3) Wellard, S. R.; Schindler, K.; Jordan, P. W. Aurora B and C Kinases Regulate Chromosome Desynapsis and Segregation during Mouse and Human Spermatogenesis. *J. Cell Sci.* **2020**, *133*, jcs248831.

(4) Bischoff, J. R.; Plowman, G. D. The Aurora/Ipl1p Kinase Family: Regulators of Chromosome Segregation and Cytokinesis. *Trends Cell Biol.* **1999**, *9*, 454−459.

(5) Sen, S.; Katayama, H.Aurora Kinases. *Targeted Therapy of Acute Myeloid Leukemi*; Springer, 2015; pp 371−389.

(6) Fu, J.; Bian, M.; Jiang, Q.; Zhang, C. Roles of Aurora Kinases in Mitosis and Tumorigenesis. *Mol. Cancer Res.* **2007**, *5*, 1−10.

(7) Warner, S. L.; Bearss, D. J.; Han, H.; Von Hoff, D. D. Targeting Aurora-2 Kinase in Cancer. *Mol. Cancer Ther.* **2003**, *2*, 589−595.

(8) Wang, X.; Zhou, Y. X.; Qiao, W.; Tominaga, Y.; Ouchi, M.; Ouchi, T.; Deng, C. X. Overexpression of Aurora Kinase A in Mouse Mammary Epithelium Induces Genetic Instability Preceding Mammary Tumor Formation. *Oncogene* **2006**, *25*, 7148−7158.

(9) Lin, Y. S.; Su, L. J.; Yu, C. T. R.; Wong, F. H.; Yeh, H. H.; Chen, S. L.; Wu, J. C.; Lin, W. J.; Shiue, Y. L.; Liu, H. S.; Hsu, S. L.; Lai, J. M.; Huang, C. Y. F. Gene Expression Profiles of the Aurora Family Kinases. *Gene Expr.* **2006**, *13*, 15−26.

(10) Marumoto, T.; Zhang, D.; Saya, H. Aurora-A - A guardian of poles. *Nat. Rev. Cancer* **2005**, *5*, 42−50.

(11) Sun, J.; Knickelbein, K.; He, K.; Chen, D.; Dudgeon, C.; Shu, Y.; Yu, J.; Zhang, L. Aurora Kinase Inhibition Induces PUMA via NF-KB to Kill Colon Cancer Cells. *Mol. Cancer Ther.* **2014**, *13*, 1298−1308.

(12) Yang, G.; Chang, B.; Yang, F.; Guo, X.; Cai, K. Q.; Xiao, X.; Wang, H.; Sen, S.; Hung, M. C.; Mills, G. B.; Chang, S.; Multani, A. S.; Mercado-Uribe, I.; Liu, J. Aurora Kinase A Promotes Ovarian Tumorigenesis through Dysregulation of the Cell Cycle and Suppression of BRCA2. *Clin. Cancer Res.* **2010**, *16*, 3171−3181.
(13) Zhou, H.; Kuang, J.; Zhong, L.; Kuo, W. L.; Gray, J. W.; Sahin, A.; Brinkley, B. R.; Sen, S. Tumour Amplified Kinase STK15/BTAK Induces Centrosome Amplification, Aneuploidy and Transformation. *Nat. Genet.* **1998**, *20*, 189−193.
(14) Chung, C. M.; Man, C.; Jin, Y.; Jin, C.; Guan, X. Y.; Wang, Q.; Wan, T. S. K.; Cheung, A. L. M.; Tsao, S. W. Amplification and Overexpression of Aurora Kinase A (AURKA) in Immortalized Human Ovarian Epithelial (HOSE) Cells. *Mol. Carcinog.* **2005**, *43*, 165−174.
(15) Gritsko, T. M.; Coppola, D.; Paciga, J. E.; Yang, L.; Sun, M.; Shelley, S. A.; Fiorica, J. V.; Nicosia, S. V.; Cheng, J. Q. Activation and Overexpression of Centrosome Kinase BTAK/Aurora-A in Human Ovarian Cancer. *Clin. Cancer Res.* **2003**, *9*, 1420−1426.
(16) Mortlock, A.; Keen, N.; Jung, F.; Heron, N.; Wilkinson, R.; Green, S. Progress in the Development of Selective Inhibitors of Aurora Kinases. *Curr. Top. Med. Chem.* **2005**, *5*, 807−821.
(17) Burum-Auensen, E.; Angelis, P. M. D.; Schjølberg, A. R.; Kravik, K. L.; Aure, M.; Clausen, O. P. F. Subcellular Localization of the Spindle Proteins Aurora A, Mad2, and BUBR1 Assessed by Immunohistochemistry. *J. Histochem. Cytochem.* **2007**, *55*, 477−486.
(18) Sogutlu, F.; Kayabasi, C.; Yelken, B. O.; Asik, A.; Gasimli, R.; Kipcak, S.; Susluer, S. Y.; Avci, C. B.; Gunduz, C. The Evaluation of Effect of Aurora Kinase Inhibitor CCT137690 in Melanoma and Melanoma Cancer Stem Cell. *Anticancer Agents Med. Chem.* **2021**, *21*, 1564−1574.
(19) Shang, Y. Y.; Yao, M.; Zhou, Z. W.; Hu, R. Y.; Yu, Y. Y.; Liu, Y. X.; Dang, J.; Zhou, S. F. Alisertib Promotes Apoptosis and Autophagy in Melanoma through P38 MAPK-Mediated Aurora a Signaling. *Oncotarget* **2017**, *8*, 107076−107088.
(20) Rajendran, V.; Gopalakrishnan, C.; Purohit, R. Impact of Point Mutation P29S in RAC1 on Tumorigenesis. *Tumor Biol.* **2016**, *37*, 15293−15304.
(21) Zhang, J.; Lin, X.; Wu, L.; Huang, J. J.; Jiang, W. Q.; Kipps, T. J.; Zhang, S. Aurora B Induces Epithelial−Mesenchymal Transition by Stabilizing Snail1 to Promote Basal-like Breast Cancer Metastasis. *Oncogene* **2020**, *39*, 2550−2567.
(22) Wu, J.; Cheng, Z.; Xu, X.; Fu, J.; Wang, K.; Liu, T.; Wu, C.; Kong, X.; Yang, Q.; Yan, G.; Zhou, H. Aurora - A Induces Chemoresistance through Activation of the Akt/Mtor Pathway in Endometrial Cancer. *Front. Oncol.* **2019**, *9*, 422.
(23) Carmena, M.; Earnshaw, W. C. The Cellular Geography of Aurora Kinases. *Nat. Rev. Mol. Cell Biol.* **2003**, *4*, 842−854.
(24) Cheetham, G. M. T.; Knegtel, R. M. A.; Coll, J. T.; Renwick, S. B.; Swenson, L.; Weber, P.; Lippke, J. A.; Austen, D. A. Crystal Structure of Aurora-2, an Oncogenic Serine/Threonine Kinase. *J. Biol. Chem.* **2002**, *277*, 42419−42422.
(25) Yan, A.; Wang, L.; Xu, S.; Xu, J. Aurora-A Kinase Inhibitor Scaffolds and Binding Modes. *Drug Discovery Today* **2011**, *16*, 260−269.
(26) Fancelli, D.; Berta, D.; Bindi, S.; Cameron, A.; Cappella, P.; Carpinelli, P.; Catana, C.; Forte, B.; Giordano, P.; Giorgini, M. L.; Mantegani, S.; Marsiglio, A.; Meroni, M.; Moll, J.; Pittalà, V.; Roletto, F.; Severino, D.; Soncini, C.; Storici, P.; Tonani, R.; Varasi, M.; Vulpetti, A.; Vianello, P. Potent and Selective Aurora Inhibitors Identified by the Expansion of a Novel Scaffold for Protein Kinase Inhibition. *J. Med. Chem.* **2005**, *48*, 3080−3084.
(27) de Groot, C. O.; Hsia, J. E.; Anzola, J. V.; Motamedi, A.; Yoon, M.; Wong, Y. L.; Jenkins, D.; Lee, H. J.; Martinez, M. B.; Davis, R. L.; Gahman, T. C.; Desai, A.; Shiau, A. K. A Cell Biologist's Field Guide to Aurora Kinase Inhibitors. *Front. Oncol.* **2015**, *5*, 285.
(28) Sarvagalla, S.; Coumar, M. Structural Biology Insight for the Design of Sub-Type Selective Aurora Kinase Inhibitors. *Curr. Cancer Drug Targets* **2015**, *15*, 375−393.
(29) Myrianthopoulos, V.; Magiatis, P.; Ferandin, Y.; Skaltsounis, A. L.; Meijer, L.; Mikros, E. An Integrated Computational Approach to the Phenomenon of Potent and Selective Inhibition of Aurora Kinases B and C by a Series of 7-Substituted Indirubins. *J. Med. Chem.* **2007**, *50*, 4027−4037.
(30) Bavetsias, V.; Linardopoulos, S. Aurora Kinase Inhibitors: Current Status and Outlook. *Front. Oncol.* **2015**, *5*, 278.
(31) Shchekotikhin, A. E.; Treshalina, H. M.; Treshchalin, M. I.; Pereverzeva, E. R.; Isakova, H. B.; Tikhomirov, A. S. Experimental Evaluation of Anticancer Efficiency and Acute Toxicity of Anthrafuran for Oral Administration. *Pharmaceuticals* **2020**, *13*, 81.
(32) Shchekotikhin, A. E.; Makarov, I. G.; Buyanov, V. N.; Preobrazhenskaya, M. N. Heterocyclic Analogs of 5,12-Naphthacenequinone. 1. Synthesis of Heterocyclic Analogs Starting from 2,3-Diaminoquinizarine. *Chem. Heterocycl. Compd.* **2005**, *41*, 914−920.
(33) Masuda, M.; Takakura, A.; Masuda, N. Next-Generation Anthracycline for the Management of Small Cell Lung Cancer: Focus on Amrubicin. *Drug Des., Dev. Ther.* **2008**, *2*, 189−192.
(34) Volodina, Y. L.; Dezhenkova, L. G.; Tikhomirov, A. S.; Tatarskiy, V. V.; Kaluzhny, D. N.; Moisenovich, A. M.; Moisenovich, M. M.; Isagulieva, A. K.; Shtil, A. A.; Tsvetkov, V. B.; Shchekotikhin, A. E. New Anthra[2,3-b]Furancarboxamides: A Role of Positioning of the Carboxamide Moiety in Antitumor Properties. *Eur. J. Med. Chem.* **2019**, *165*, 31−45.
(35) Yaoxian, W.; Hui, Y.; Yunyan, Z.; Yanqin, L.; Xin, G.; Xiaoke, W. Emodin Induces Apoptosis of Human Cervical Cancer Hela Cells via Intrinsic Mitochondrial and Extrinsic Death Receptor Pathway. *Cancer Cell Int.* **2013**, *13*, 71.
(36) Fukuhara, K.; Oikawa, S.; Hakoda, N.; Sakai, Y.; Hiraku, Y.; Shoda, T.; Saito, S.; Miyata, N.; Kawanishi, S.; Okuda, H. 9-Nitroanthracene Derivative as a Precursor of Anthraquinone for Photodynamic Therapy. *Bioorg. Med. Chem.* **2007**, *15*, 3869−3873.
(37) Shchekotikhin, A. E.; Dezhenkova, L. G.; Tsvetkov, V. B.; Luzikov, Y. N.; Volodina, Y. L.; Tatarskiy, V. V.; Kalinina, A. A.; Treshalin, M. I.; Treshalina, H. M.; Romanenko, V. I.; Kaluzhny, D. N.; Kubbutat, M.; Schols, D.; Pommier, Y.; Shtil, A. A.; Preobrazhenskaya, M. N. Discovery of Antitumor Anthra[2,3-b]Furan-3-Carboxamides: Optimization of Synthesis and Evaluation of Antitumor Properties. *Eur. J. Med. Chem.* **2016**, *112*, 114−129.
(38) Singh, M.; Malhotra, L.; Haque, M. A.; Kumar, M.; Tikhomirov, A.; Litvinova, V.; Korolev, A. M.; Ethayathulla, A. S.; Das, U.; Shchekotikhin, A. E.; Kaur, P. Heteroarene-Fused Anthraquinone Derivatives as Potential Modulators for Human Aurora Kinase B. *Biochimie* **2021**, *182*, 152−165.
(39) Pereverzeva, E. R.; Treschalin, M. I.; Eremkin, N. V.; Shchekotikhin, A. E.; Treschalin, I. D. Toxicological Characteristic of Novel Antitumour Multitargeted Agent Anthrafuran. *Russ. J. Biother.* **2017**, *16*, 80.
(40) Aliagas-Martin, I.; Burdick, D.; Corson, L.; Dotson, J.; Drummond, J.; Fields, C.; Huang, O. W.; Hunsaker, T.; Kleinheinz, T.; Krueger, E.; Liang, J.; Moffat, J.; Phillips, G.; Pulk, R.; Rawson, T. E.; Ultsch, M.; Walker, L.; Wiesmann, C.; Zhang, B.; Zhu, B. Y.; Cochran, A. G. A Class of 2,4-Bisanilinopyrimidine Aurora A Inhibitors with Unusually High Selectivity against Aurora B. *J. Med. Chem.* **2009**, *52*, 3300−3307.
(41) Schrödinger. *Maestro Schrödinger. Schrödinger Release 2018-1*; Schrödinger, 2018.
(42) Schrödinger. *Protein Preparation Wizard*; Schrödinger, 2011.
(43) ChemAxon. *Marvin Sketch*; ChemAxon, 2012.
(44) O'Boyle, N. M.; Banck, M.; James, C. A.; Morley, C.; Vandermeersch, T.; Hutchison, G. R. Open Babel: An Open Chemical Toolbox. *J. Cheminf.* **2011**, *3*, 33.
(45) Schrödinger. *LigPrep Schrödinger. Schrödinger Release 2018-1*; Schrödinger, 2018.
(46) Friesner, R. A.; Murphy, R. B.; Repasky, M. P.; Frye, L. L.; Greenwood, J. R.; Halgren, T. A.; Sanschagrin, P. C.; Mainz, D. T. Extra Precision Glide: Docking and Scoring Incorporating a Model of Hydrophobic Enclosure for Protein-Ligand Complexes. *J. Med. Chem.* **2006**, *49*, 6177−6196.

https://doi.org/10.1021/acsomega.2c00740
ACS Omega 2022, 7, 39603−39618

(47) Schrödinger. *Schrödinger Release 2018-1. Maestro-Desmond Interoperability Tools, Desmond Molecular Dynamics System*; Schrödinger, 2018.
(48) Berendsen, H. J. C.; Postma, J. P. M.; Van Gunsteren, W. F.; Dinola, A.; Haak, J. R. Molecular Dynamics with Coupling to an External Bath. *J. Chem. Phys.* **1984**, *76* (2662), 3684−3690.
(49) Brown, D.; Clarke, J. H. R. A Loose-Coupling, Constant-Pressure, Molecular Dynamics Algorithm for Use in the Modelling of Polymer Materials. *Comput. Phys. Commun.* **1991**, *62* (360), 3628−3631.
(50) Eslami, H.; Mozaffari, F.; Moghadasi, J.; Müller-Plathe, F. Molecular Dynamics Simulation of Confined Fluids in Isosurface-Isothermal- Isobaric Ensemble. *J. Chem. Phys.* **2008**, *129*, 194702.
(51) Shinoda, W.; Mikami, M. Rigid-Body Dynamics in the Isothermal-Isobaric Ensemble: A Test on the Accuracy and Computational Efficiency. *J. Comput. Chem.* **2003**, *24*, 920−930.
(52) Martyna, G. J.; Klein, M. L.; Tuckerman, M. Nosé-Hoover Chains: The Canonical Ensemble via Continuous Dynamics. *J. Chem. Phys.* **1992**, *97*, 2635−2643.
(53) Cheng, A.; Merz, K. M. Application of the Nosé-Hoover Chain Algorithm to the Study of Protein Dynamics. *J. Phys. Chem.* **1996**, *5* (1393), 1927−1937.
(54) Martyna, G. J.; Tobias, D. J.; Klein, M. L. Constant Pressure Molecular Dynamics Algorithms. *J. Chem. Phys.* **1994**, *101*, 4177−4189.
(55) Procacci, P.; Berne, B. J. Computer Simulation of Solid C60 Using Multiple Time-Step Algorithms. *J. Chem. Phys.* **1994**, *101*, 2421−2431.
(56) Lu, C.; Wu, C.; Ghoreishi, D.; Chen, W.; Wang, L.; Damm, W.; Ross, G. A.; Dahlgren, M. K.; Russell, E.; Von Bargen, C. D.; Abel, R.; Friesner, R. A.; Harder, E. D. OPLS4: Improving Force Field Accuracy on Challenging Regimes of Chemical Space. *J. Chem. Theory Comput.* **2021**, *17* (7), 4291−4300.
(57) Darden, T.; York, D.; Pedersen, L. Particle Mesh Ewald: An N·log(N) Method for Ewald Sums in Large Systems. *J. Chem. Phys.* **1993**, *98*, 10089−10092.
(58) Wells, B. A.; Chaffee, A. L. Ewald Summation for Molecular Simulations. *J. Chem. Theory Comput.* **2015**, *11*, 3684−3695.
(59) Zhang, X.; Perez-Sanchez, H.; Lightstone, F. A Comprehensive Docking and MM/GBSA Rescoring Study of Ligand Recognition upon Binding Antithrombin. *Curr. Top. Med. Chem.* **2017**, *17*, 1631−1639.
(60) Forouzesh, N.; Mishra, N. An Effective MM/GBSA Protocol for Absolute Binding Free Energy Calculations: A Case Study on SARS-CoV-2 Spike Protein and the Human ACE2 Receptor. *Molecules* **2021**, *26*, 2383.
(61) Shchekotikhin, A. E.; Luzikov, Y. N.; Sinkevich, Y. B.; Buyanov, V. N.; Preobrazhenskaya, M. N. Heterocyclic Analogs of 5,12-Naphthacenequinone 7*. Synthesis of Naphtho-[2,3-f]Isatin-5,10-Dione Derivatives. *Chem. Heterocycl. Compd.* **2008**, *44*, 1245−1249.
(62) Cogoi, S.; Zorzet, S.; Shchekotikhin, A. E.; Xodo, L. E. Potent Apoptotic Response Induced by Chloroacetamidine Anthrathiophenediones in Bladder Cancer Cells. *J. Med. Chem.* **2015**, *58*, 5476−5485.
(63) Concepcion, J.; Witte, K.; Wartchow, C.; Choo, S.; Yao, D.; Persson, H.; Wei, J.; Li, P.; Heidecker, B.; Ma, W.; Varma, R.; Zhao, L.-S.; Perillat, D.; Carricato, G.; Recknor, M.; Du, K.; Ho, H.; Ellis, T.; Gamez, J.; Howes, M.; Phi-Wilson, J.; Lockard, S.; Zuk, R.; Tan, H. Label-Free Detection of Biomolecular Interactions Using BioLayer Interferometry for Kinetic Characterization. *Comb. Chem. High Throughput Screen.* **2009**, *12*, 791−800.
(64) Soncini, C.; Carpinelli, P.; Gianellini, L.; Fancelli, D.; Vianello, P.; Rusconi, L.; Storici, P.; Zugnoni, P.; Pesenti, E.; Croci, V.; Ceruti, R.; Giorgini, M. L.; Cappella, P.; Ballinari, D.; Sola, F.; Varasi, M.; Bravo, R.; Moll, J. PHA-680632, a Novel Aurora Kinase Inhibitor with Potent Antitumoral Activity. *Clin. Cancer Res.* **2006**, *12*, 4080−4089.
(65) Kuzmanic, A.; Zagrovic, B. Determination of Ensemble-Average Pairwise Root Mean-Square Deviation from Experimental B-Factors. *Biophys. J.* **2010**, *98*, 861−871.
(66) Sargsyan, K.; Grauffel, C.; Lim, C. How Molecular Size Impacts RMSD Applications in Molecular Dynamics Simulations. *J. Chem. Theory Comput.* **2017**, *13*, 1518−1524.
(67) Talele, T. T.; McLaughlin, M. L. Molecular Docking/Dynamics Studies of Aurora A Kinase Inhibitors. *J. Mol. Graph. Model.* **2008**, *26*, 1213−1222.
(68) Tari, L. W.; Hoffman, I. D.; Bensen, D. C.; Hunter, M. J.; Nix, J.; Nelson, K. J.; McRee, D. E.; Swanson, R. V. Structural Basis for the Inhibition of Aurora A Kinase by a Novel Class of High Affinity Disubstituted Pyrimidine Inhibitors. *Bioorg. Med. Chem. Lett* **2007**, *17*, 688−691.
(69) Sharma, J.; Bhardwaj, V. K.; Das, P.; Purohit, R. Identification of Naturally Originated Molecules as γ-Aminobutyric Acid Receptor Antagonist. *J. Biomol. Struct. Dyn.* **2021**, *39*, 911−922.
(70) Akbar, S. M. D.; Sreeramulu, K.; Sharma, H. C. Tryptophan Fluorescence Quenching as a Binding Assay to Monitor Protein Conformation Changes in the Membrane of Intact Mitochondria. *J. Bioenerg. Biomembr.* **2016**, *48*, 241−247.
(71) Sindrewicz, P.; Li, X.; Yates, E. A.; Turnbull, J. E.; Lian, L. Y.; Yu, L. G. Intrinsic Tryptophan Fluorescence Spectroscopy Reliably Determines Galectin-Ligand Interactions. *Sci. Rep.* **2019**, *9*, 11851.
(72) Nguyen, T. D.; Jeong, K.; Ryu, J.; Jung, C. H. A Rapid Screening of Ligand Binding by Measuring Intrinsic Fluorescence Changes of Proteins. *Bull. Korean Chem. Soc.* **2017**, *38*, 1028−1032.
(73) Lakowicz, J. R.; Masters, B. R.*Principles of Fluorescence Spectroscopy*, 3rd ed.; Springer, 2008.
(74) Badrinarayan, P.; Sastry, G. N. Specificity Rendering 'Hot-Spots' for Aurora Kinase Inhibitor Design: The Role of Non-Covalent Interactions and Conformational Transitions. *PLoS One* **2014**, *9*, No. e113773.
(75) Schulze, J. O.; Saladino, G.; Busschots, K.; Neimanis, S.; Süß, E.; Odadzic, D.; Zeuzem, S.; Hindie, V.; Herbrand, A. K.; Lisa, M. N.; Alzari, P. M.; Gervasio, F. L.; Biondi, R. M. Bidirectional Allosteric Communication between the ATP-Binding Site and the Regulatory PIF Pocket in PDK1 Protein Kinase. *Cell Chem. Biol.* **2016**, *23*, 1193−1205.
(76) Liewer, S.; Huddleston, A. Alisertib: A Review of Pharmacokinetics, Efficacy and Toxicity in Patients with Hematologic Malignancies and Solid Tumors. *Expert Opin. Invest. Drugs* **2018**, *27*, 105−112.
(77) Tsuchiya, Y.; Byrne, D. P.; Burgess, S. G.; Bormann, J.; Baković, J.; Huang, Y.; Zhyvoloup, A.; Yu, B. Y. K.; Peak-Chew, S.; Tran, T.; Bellany, F.; Tabor, A. B.; Chan, A. E.; Guruprasad, L.; Garifulin, O.; Filonenko, V.; Vonderach, M.; Ferries, S.; Eyers, C. E.; Carroll, J.; Skehel, M.; Bayliss, R.; Eyers, P. A.; Gout, I. Covalent Aurora A Regulation by the Metabolic Integrator Coenzyme A. *Redox Biol.* **2020**, *28*, 101318.
(78) Janeček, M.; Rossmann, M.; Sharma, P.; Emery, A.; Huggins, D. J.; Stockwell, S. R.; Stokes, J. E.; Tan, Y. S.; Almeida, E. G.; Hardwick, B.; Narvaez, A. J.; Hyvönen, M.; Spring, D. R.; McKenzie, G. J.; Venkitaraman, A. R. Allosteric Modulation of AURKA Kinase Activity by a Small-Molecule Inhibitor of Its Protein-Protein Interaction with TPX2. *Sci. Rep.* **2016**, *6*, 28528.
(79) Young, M. A.; Shah, N. P.; Chao, L. H.; Seeliger, M.; Milanov, Z. V.; Biggs, W. H.; Treiber, D. K.; Patel, H. K.; Zarrinkar, P. P.; Lockhart, D. J.; Sawyers, C. L.; Kuriyan, J. Structure of the Kinase Domain of an Imatinib-Resistant Abl Mutant in Complex with the Aurora Kinase Inhibitor VX-680. *Cancer Res.* **2006**, *66*, 1007−1014.
(80) Tikhomirov, A.; Shtil, A.; Shchekotikhin, A. Advances In the Discovery of Anthraquinone-Based Anticancer Agents. *Recent Pat. Anticancer. Drug Discov.* **2017**, *13*, 159.
(81) Garuti, L.; Roberti, M.; Bottegoni, G. Small Molecule Aurora Kinases Inhibitors. *Curr. Med. Chem.* **2009**, *16*, 1949.
(82) Malik, M. S.; Alsantali, R. I.; Jassas, R. S.; Alsimaree, A. A.; Syed, R.; Alsharif, M. A.; Kalpana, K.; Morad, M.; Althagafi, I. I.; Ahmed, S. A. Journey of Anthraquinones as Anticancer Agents-a Systematic Review of Recent Literature. *RSC Adv.* **2021**, *11*, 35806.
(83) Gupta, D.; Kumar, M.; Singh, M.; Salman, M.; Das, U.; Kaur, P. Identification of Polypharmacological Anticancerous Molecules

https://doi.org/10.1021/acsomega.2c00740
ACS Omega 2022, 7, 39603−39618

against Aurora Kinase Family of Proteins. *J. Cell. Biochem.* **2022**, *123*, 719.

https://doi.org/10.1021/acsomega.2c00740
ACS Omega 2022, 7, 39603−39618